Structural, elastic, vibrational and electronic properties of amorphous Al_2O_3 from *ab initio* calculations

2011 J. Phys.: Condens. Matter 23 495401

(http://iopscience.iop.org/0953-8984/23/49/495401)

IOP PUBLISHING JOURNAL OF PHYSICS: CONDENSED MATTER
J. Phys.: Condens. Matter **23** (2011) 495401 (8pp) doi:10.1088/0953-8984/23/49/495401

Structural, elastic, vibrational and electronic properties of amorphous Al_2O_3 from *ab initio* calculations

Sergio Davis[1] **and Gonzalo Gutiérrez**[2]

Grupo de Nanomateriales, Departamento de Física, Facultad de Ciencias, Universidad de Chile, Casilla 653, Santiago, Chile

E-mail: sdavis@gnm.cl and gonzalo@fisica.ciencias.uchile.cl

Received 13 April 2011, in final form 20 October 2011
Published 18 November 2011
Online at stacks.iop.org/JPhysCM/23/495401

Abstract
First-principles molecular dynamics calculations of the structural, elastic, vibrational and electronic properties of amorphous Al_2O_3, in a system consisting of a supercell of 80 atoms, are reported. A detailed analysis of the interatomic correlations allows us to conclude that the short-range order is mainly composed of AlO_4 tetrahedra, but, in contrast with previous results, also an important number of AlO_6 octahedra and AlO_5 units are present. The vibrational density of states presents two frequency bands, related to bond-bending and bond-stretching modes. It also shows other recognizable features present in similar amorphous oxides. We also present the calculation of elastic properties (bulk modulus and shear modulus). The calculated electronic structure of the material, including total and partial electronic density of states, charge distribution, electron localization function and the ionicity for each species, gives evidence of correlation between the ionicity and the coordination for each Al atom.

(Some figures may appear in colour only in the online journal)

1. Introduction

Among amorphous solids, amorphous aluminum oxide (Al_2O_3) or alumina [1] stands out due to its technological applications, mainly as an insulator substrate in the fabrication of electronic components [2, 3] and recently as a support for nanoparticles in multilayered heterostructures [4]. Al_2O_3 in its different phases is also relevant as a material outside Earth, in astronomy and astrophysics [5–7].

Knowledge of the microscopic structure of amorphous Al_2O_3 can reveal key information about the oxidation and passivation processes in Al, as well as a better comprehension of the origin of its excellent macroscopic properties. Its structure has been studied experimentally using several techniques: x-ray diffraction [8], EXAFS (extended x-ray absorption fine structure) and EXELFS (electron extended energy loss fine structure) [9], x-ray and neutron diffraction [10], and recently using solid-state NMR [11, 12]. In these studies, only the first two diffraction peaks of the crystalline solid remain, clear evidence of its lack of long-range ordering.

It has also been found that aluminum nanoclusters in low-density oxygen gas at room temperature can form layers of thin alumina films [13]. Such films have a rather complex amorphous structure, and a knowledge of its electronic structure would be an important step toward understanding the detailed mechanism of the oxidation and passivation process.

The application of alumina to micro-electronics and thin film devices takes into account its electronic properties. In particular, the band gap has been the subject of discussion in the case of thin alumina films. So far, there is no clear explanation of the decrease of the energy band gap value reported for thin α-alumina and γ-alumina films. It has been argued that this could be due to the appearance of a metallic characteristic in the alumina surface layers, or to some defect

[1] www.gnm.cl/~sdavis.
[2] http://fisica.ciencias.uchile.cl/~gonzalo.

levels located in the band gap [14]. Recently amorphous alumina, because of its high dielectric constant, has also been proposed for the next generation of electronic devices [15].

In this work, we present a study of structural, electronic, elastic and dynamical properties of amorphous Al_2O_3, obtained by combining classical and *ab initio* molecular dynamics (MD). The preparation of the liquid sample, quenching and equilibration of the amorphous solid were done using classical MD, and the final configuration from this process was used as input for the *ab initio* MD. This is the same methodology used for SiO_2 by Benoit *et al* [16], and in the same spirit as the one used by Giacomazzi *et al* [17], giving reliable results depending on the quality of the interatomic potential chosen for the preparation.

2. Method

The model structure of amorphous alumina was obtained by the combined use of classical and *ab initio* MD simulations. The 'quench from the melt' technique (as described by Gutiérrez *et al* [18]) was used to obtain an amorphous sample (composed of 80 atoms, 32Al + 48O, inside a cubic cell) at the density $\rho = 3.2$ g cm^{-3}, by quenching a liquid structure at the same density. We use the last configuration (set of atomic coordinates) from this procedure as the starting configuration for the *ab initio* runs.

All the classical MD simulations were performed in the microcanonical ensemble using a pairwise interatomic potential [19], which has been shown to reproduce a number of experimental properties for crystals [20], liquid [21] and amorphous phases [18]. This amorphous sample was simulated for more than 30 000 time steps in the Born–Oppenheimer *ab initio* MD as is implemented in the VASP package [22, 23]. The simulation was done in the framework of DFT within the local density approximation (LDA) [24]. The exchange–correlation potential was approximated by the Perdew–Zunger [25] parameterization of the LDA. The valence wavefunctions were expanded at the Γ point of the supercell in plane waves, using a cutoff of 296.77 eV. The core electrons were replaced by the ultrasoft pseudopotentials supplied in the VASP package. The *ab initio* MD was also performed in the microcanonical ensemble, using periodic boundary conditions and a time step of 3 fs. The system was equilibrated during 9 ps at $T = 400$ K. The data used to calculate the structural properties were accumulated on the following 4.5 ps. In order to calculate the dynamical properties such as the velocity autocorrelation function (VACF) and the vibrational density of states, we performed a longer run, over 30 ps, using the same time step and DFT parameters.

The last configuration obtained from the *ab initio* MD runs was used to perform a complete relaxation of the atomic positions (but keeping the density fixed at 3.2 g cm^{-3}), in order to calculate in detail the electronic and elastic properties.

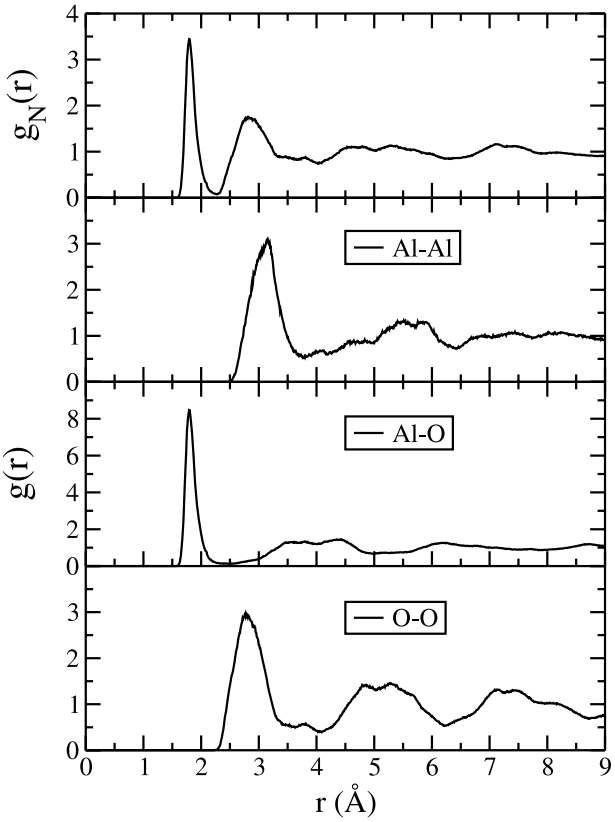

Figure 1. Total and partial pair distribution function for amorphous Al_2O_3.

3. Results

3.1. Structural properties

Structural properties were studied by examining atomic correlations described by pair distribution functions $g(r)$, coordination numbers and angular distributions. Figure 1 shows the results of partial $g_{\alpha\beta}(r)$ and total neutron-weighted pair distribution functions. From the position of the first peak in these curves we can infer the Al–Al, Al–O and O–O nearest-neighbor distances. We can see that the Al–Al nearest-neighbor distance is around 3.1 Å. In the same way, we can estimate the Al–O bond length to be 1.8 Å, and the O–O bond length 2.8 Å. These values are slightly different from the ones obtained in classical MD, but closer to the experimental ones. In particular, the Al–O bond length obtained from *ab initio* MD is in complete agreement with the experimental value of 1.8 ± 0.21 Å [10].

Interatomic distances can also be seen in reciprocal space, in terms of diffraction patterns. The neutron static scattering factor, $S_N(q)$, calculated as the Fourier transform of the partial $g_{\alpha\beta}(r)$, is shown along with the experimental results [10] in figure 2. The results of our calculations show a reasonable agreement with the diffraction data, despite the limited size of the system[3]. Here, the low q-parts are

[3] For example, the pre-peak near $q = 1.7$ Å^{-1} has been difficult to reproduce in *ab initio* simulations, due to the size limitation. Strictly speaking, values of q less than $4\pi/L$, with length cell box $L = 9.4$ Å, are not reliable. Classical MD simulations with larger systems show better agreement on this feature [18].

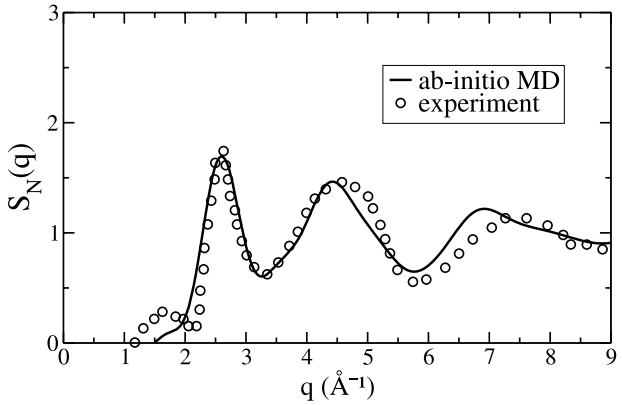

Figure 2. Calculated (solid line) and experimental (dots, [10]) neutron static structure function for amorphous Al_2O_3.

related to intermediate-range order, while the first peak at $q = 2.5$ Å^{-1} comes from nearest-neighbor Al–Al, Al–O and O–O correlations.

Figure 3 shows histograms for the coordination numbers. We can see that almost 50% of Al atoms have tetrahedral coordination, but more than 40% have fivefold coordination. These results are in contrast with previous classical MD simulations [18, 26, 27], where the great majority of Al atoms have coordination four [28], and also with recent MD simulations of amorphous Y_2O_3–Al_2O_3 [29], where an average Al–O coordination of 4.9 ± 0.2 is found. The coordination number of O–Al atoms is sharply defined, being most O atoms surrounded by three Al atoms, unlike the Al–Al and O–O coordinations, which as in the case of classical MD are rather broad, showing maxima for 8 and 9 in Al–Al and 11 and 12 for O–O. If we integrate the first peak of $g_{\alpha\beta}(r)$ up to a cutoff distance $R_{\alpha\beta}$ (close to the first minima), we obtain the average coordination number, which corresponds to 4.6 for Al–O, 3.1 for O–Al, 8.7 for Al–Al and 11.1 and for O–O. As can be seen, for the case of the Al–O coordination, the obtained average value is 4.62, closer to fivefold coordination than to fourfold. Interestingly, recent work by Jahn and Madden [30] using a polarizable model in classical MD predicts a higher Al–O average coordination number of approximately 4.5, very close to our *ab initio* estimate.

The bond-angle distribution in amorphous Al_2O_3 is depicted in figure 4. The expected angles in a AlO_4 tetrahedron, O–Al–O = 109.5°, O–O–O = 60° and Al–O–O = 35.3° are all predominant in these angle distributions. This leads to the conclusion that such a tetrahedron is one of the basic units in the local amorphous structure, as reported in [18]. But, interestingly, in contrast to previous classical MD simulations [18, 26, 27], the O–Al–O angle distribution also presents a peak around 85°. This piece of information, together with the fact that the average Al–O coordination number is higher than four, and the Al–O bond length is higher than in classical MD, suggests that a certain proportion of distorted AlO_5 and AlO_6 octahedra are also present. Both structures are depicted in figure 5.

Regarding the structure beyond the short-range order, we can obtain information about the way the basic building blocks are linked together by examining the Al–O–Al angle distribution. From this we see that the basic units, tetrahedra and distorted octahedra, are linked together not only at 120°, as obtained from classical MD, but also around 95°. This

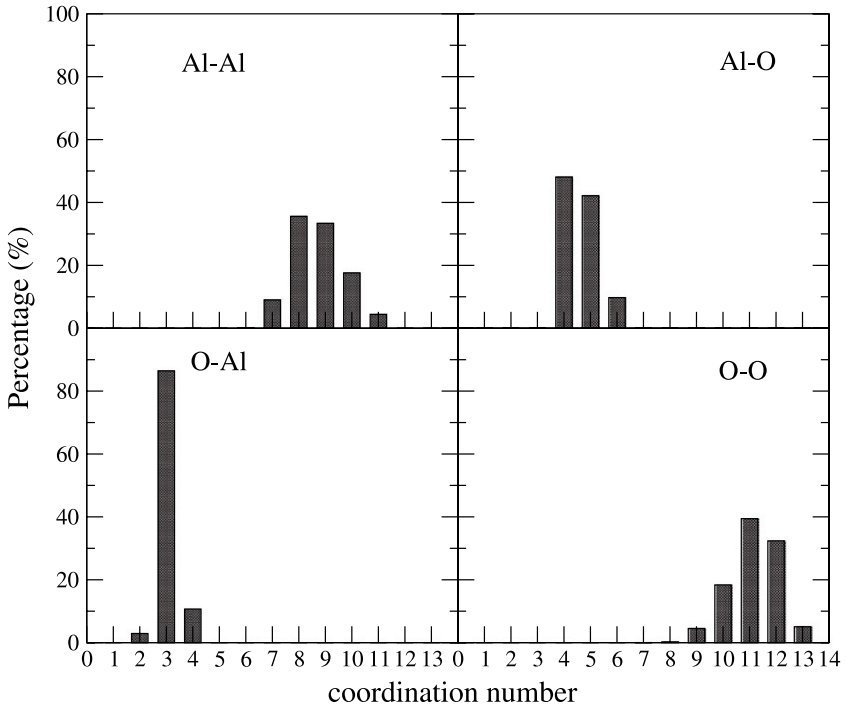

Figure 3. Nearest-neighbor distribution for amorphous Al_2O_3.

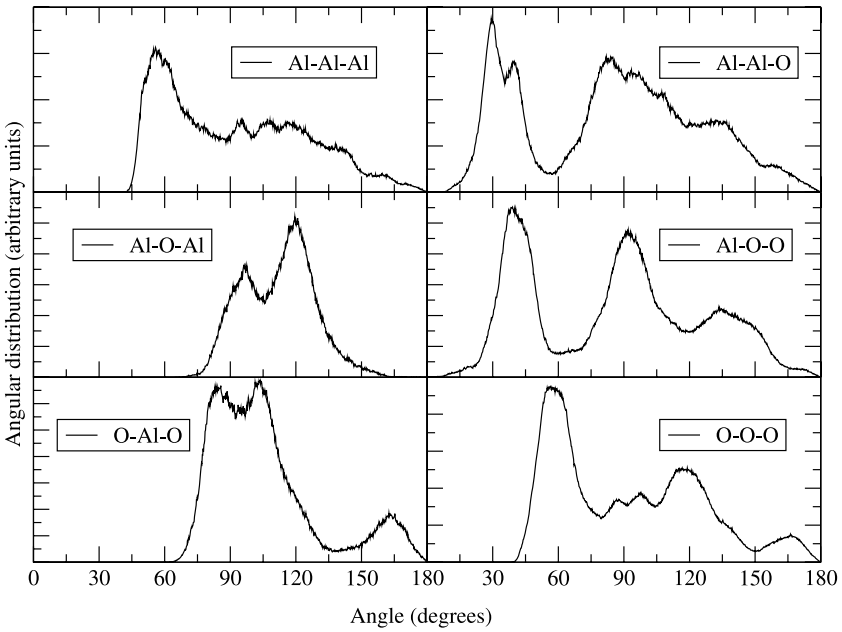

Figure 4. Angular distribution for amorphous Al_2O_3.

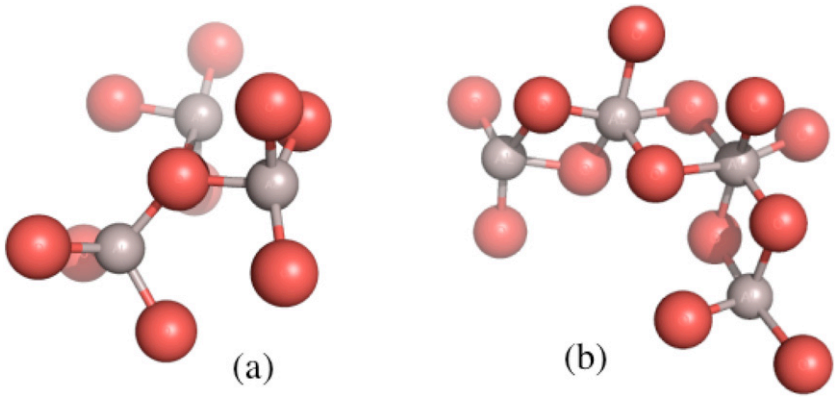

Figure 5. Structural units and their connectivity for amorphous Al_2O_3, according to the *ab initio* MD simulation. (a) Corner-sharing tetrahedra, (b) edge-sharing polyhedra. Large spheres represent oxygen atoms and small ones aluminum atoms.

can be interpreted as linking not only by corners, but also by sharing edges and faces, as shown in figure 6.

3.2. Elastic properties

In order to compute the elastic properties we performed a complete structural relaxation, at a density of 3.2 g cm^{-3}. The energy–volume curve is shown in figure 7, together with the corresponding Birch–Murnaghan fit [31]. From this we obtained a bulk modulus $B_0 = 193.41$ GPa, and an equilibrium density of 3.37 g cm^{-3}. We have also calculated the shear modulus G by subjecting the sample to small strain along one axis, obtaining a value of $G = 141$ GPa. These values are lower than the known values for alumina polymorphs. For example, the bulk modulus of γ-alumina is around 219 GPa [32].

From these values we calculated the Young's modulus as $E = 9BG/(3B + G)$ and the Poisson ratio $\nu = (3B - 2G)/2(3B+G)$. The comparison with the experimental values corresponding to α-Al_2O_3 is shown in table 1. The values for amorphous alumina are smaller than the ones for the crystalline structure. Unfortunately, as far as we know, there are no experimental data available for mechanical properties of bulk amorphous alumina. However, some measurements on anodic and porous amorphous alumina has been done recently using nanoindentation techniques, estimating a Young's modulus of about 122 GPa by Alcala *et al* for anodic amorphous alumina [33], and 140 GPa by Xia *et al* for porous amorphous alumina [34]. The difference between the calculated Young's modulus $E = 340$ GPa with respect to the experimental value, 122 GPa, as measured by nanoindentation is due to the difference in the samples considered: the model structure used here is a bulk amorphous alumina, that is, non-porous and homogeneous, whereas the experiments considered thin films of amorphous anodic alumina, which as the authors report are porous and contain a certain amount of moisture as a consequence of the anodizing process.

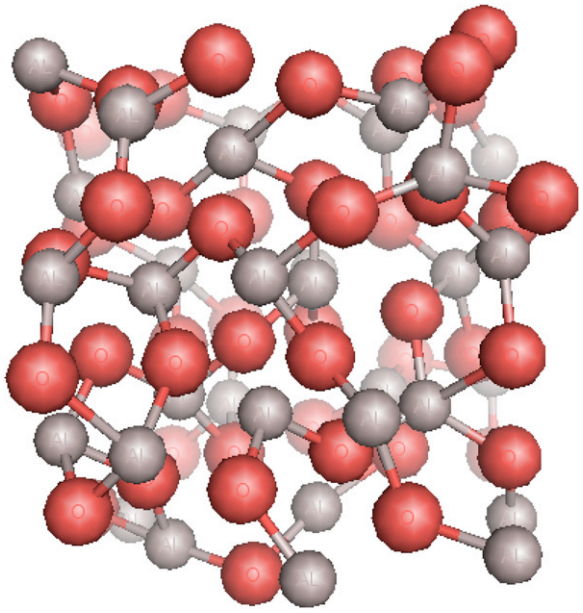

Figure 6. Snapshot of an amorphous Al_2O_3 configuration. Large spheres represent oxygen atoms, and small ones aluminum atoms.

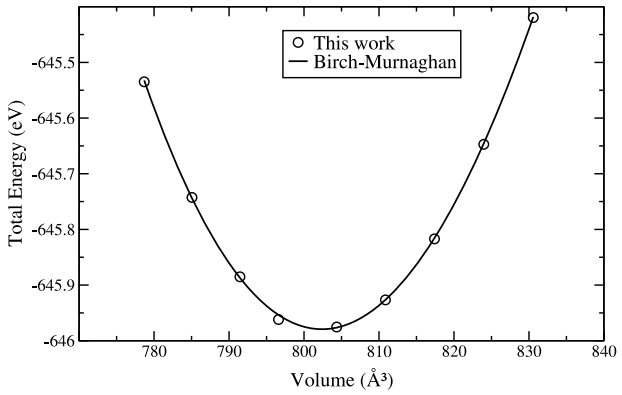

Figure 7. Energy as a function of volume for amorphous Al_2O_3, together with the corresponding Birch–Murnaghan fit.

Table 1. The isotropic bulk modulus B, shear modulus G, Young's modulus E and Poisson ratio ν of amorphous (this work) and α-Al_2O_3 (experiment).

Phase	B (GPa)	G (GPa)	E (GPa)	ν
Amorphous	193.4	141.0	340.3	0.2
α	253	164	404.6	0.23

3.3. Dynamical properties

Dynamic properties were investigated by means of the vibrational density of states (v-DOS), which is proportional to the Fourier transform of the VACF. Figure 8 shows the partial and neutron-weighted v-DOS [35] for future comparison with experiment. Several features can be distinguished from this plot. First, around 5 THz there is a 'bump', corresponding to the so-called Boson peak, a signature of the amorphous state. At high frequency, between 18 and 25 THz, there is a double peak, which is also present in the vibrational spectra

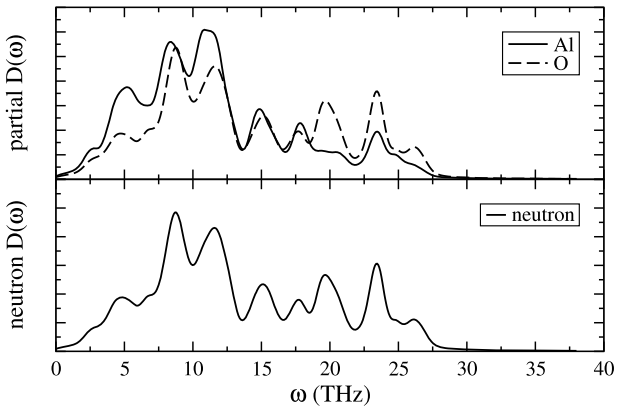

Figure 8. Partial and neutron-weighted vibrational density of states for amorphous Al_2O_3.

of amorphous SiO_2, and appeared as a general feature of an AX_2 amorphous network [36].

From the partial v-DOS, which gives the participation ratio of each species to the total density of states, we can infer that the contribution from Al atoms to the vibration modes is mainly at low frequencies, whereas the O atoms contribute more clearly at high frequencies. In this way, two main bands can be distinguished: a low frequency band up to 15–20 THz, and a higher frequency band, from 20 to 30 THz. The lower band is related to the inter-tetrahedra vibrations, whereas the higher band is associated to the intra-tetrahedra vibrations. This picture is consistent with the description given for other amorphous networks, composed mainly by a basic tetrahedron, such as amorphous SiO_2 [37] and GeO_2 [17], where the lower band is related to the bond-bending modes and the higher band is related to the bond-stretching modes.

It is interesting to compare our calculated v-DOS for amorphous Al_2O_3 with the v-DOS of its crystalline counterparts [38]. In particular, they present striking similarities with the θ-Al_2O_3 v-DOS: both spectra can be divided in two main bands, with the separation frequency around 18 THz, the lower band containing approximately 70% of the v-DOS. This is plausible, taken into account that θ-Al_2O_3 is the crystalline phase which has the higher proportion (50%) of fourfold-coordinated Al atoms.

3.4. Electronic properties

In figure 9 we show the total and partial Al and O density of states (DOS). There are three bands, the lower valence band (LVB) and the upper valence band (UVB) being dominated by oxygen states, and the conduction band composed of both Al and O states. The peak present at around 8 eV corresponds to the bottommost conduction band, because our calculation included only one **k** point, namely the Γ point. Figure 10 presents the partial, local density of states (LDOS). The conduction band (CB) is separated by a rather small gap, 2.4 eV, from the UVB. The measured bandgap [14] for amorphous thin films is 3.2 eV. The electronic states of the low valence band are dominated by O 2s states, whereas the upper valence band (UVB) is dominated by O 2p states. The

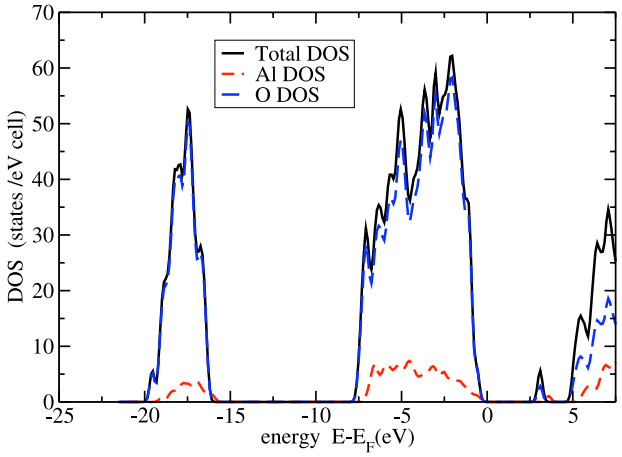

Figure 9. Total density of states (full lines), and Al and O partial density of states (dashed lines).

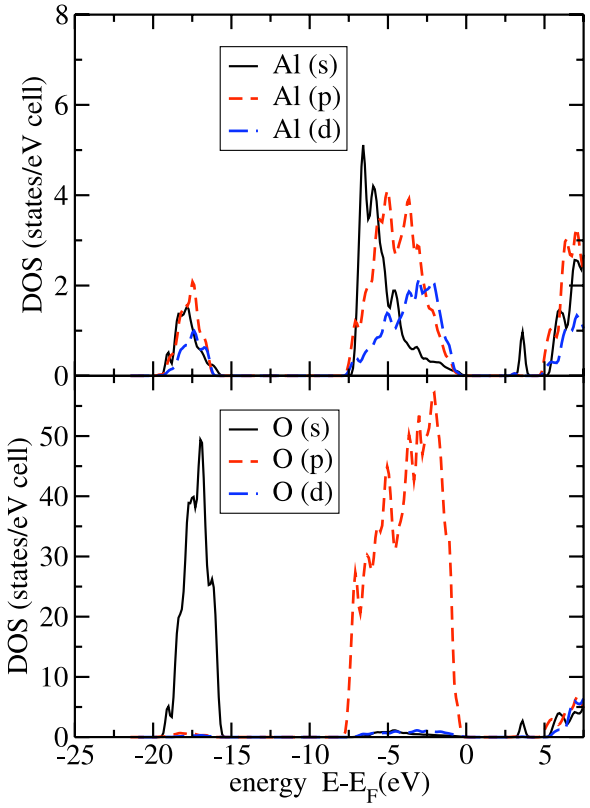

Figure 10. Partial orbital Al and O density of states.

CB is mainly composed of the Al 3s and 3p states and O 2s and 2p states. From figure 10 we can see the that 3s, 3p and 3d Al states contribute equally to the valence bands, although this contribution is rather small.

In figure 11 we present a comparison of our calculated DOS with the corresponding one of γ-alumina [32, 39], and the XPS experimental measurement [40], γ-alumina being regarded as the closer crystalline phase to amorphous alumina. The DOSs are qualitatively similar to each other, but the calculated bandgap in amorphous alumina (2.9 eV) is smaller than the calculated bandgap for γ-alumina (≈4.0 eV). Also,

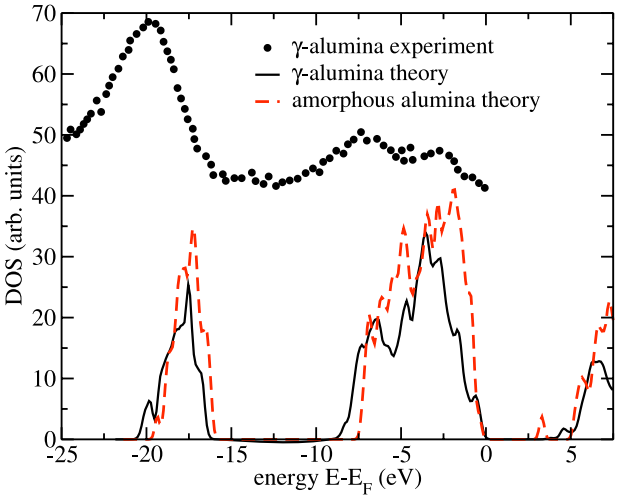

Figure 11. Experimental (XPS) electronic DOS for γ-alumina, together with *ab initio* electronic DOS for amorphous and γ-alumina.

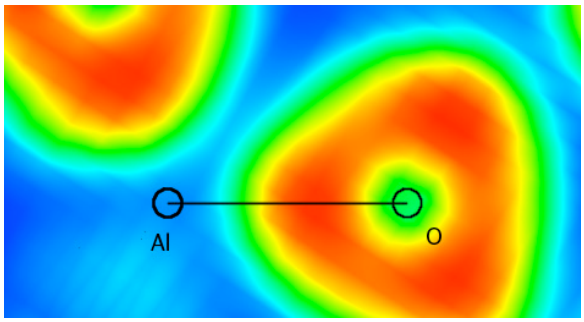

Figure 12. Electron localization function of a plane containing an Al–O bond. The magnitude is given in a color scheme in which high values correspond to red and low to blue.

both the LVB and UVB in amorphous alumina are rather narrow with respect to the ones found in γ-alumina.

We can gain further insight into the nature of the bonding by means of the electron localization function (ELF), which is presented in figures 12 and 13. The ELF is an empirical three-dimensional function [41], yielding values between 0.5 and 1.0 in regions that can be ascribed to bonding and non-bonding localized electrons (red in the figure) and values less than 0.5 where one expects the electrons to be delocalized (blue in the figure). In figures 12 and 13, the magnitude of the ELF is encoded using a color scheme in which high values correspond to red and low values to blue. Figure 12 shows a plane corresponding to an Al atom surrounded by four O atoms (one plane of an octahedrally coordinated Al atom). The location of the Al ion is at the center of the figure, and is characterized by very low charge densities, as expected of a pseudopotential calculation. Oxygen atoms are identified by large red annular regions. This electron localization around O atoms indicates a highly ionic kind of bonding. However, a small degree of covalency is present as the region of high ELF around O atoms is not spherically symmetric and exhibits lobes directed toward the Al ion.

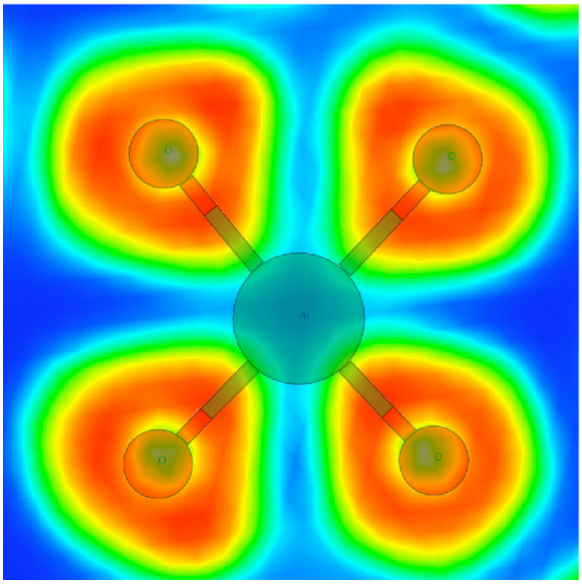

Figure 13. Electron localization function of a plane containing an Al at the center and four O in the vertex. The magnitude is given in a color scheme in which high values correspond to red and low to blue.

Table 2. Atomic charge transfer in Al and O according to their respective coordination.

Coordination	Crystal radius (Å)	Atomic charge
Al 4	0.53	2.93 ± 0.002
Al 5	0.62	2.85 ± 0.004
Al 6	0.675	2.78 ± 0.002
O 2	1.21	-1.88 ± 0.0
O 3	1.22	-1.92 ± 0.043
O 4	1.24	-1.96 ± 0.03

Quantitative information about the ionicity can be obtained by estimating the ionic charge. Following Ruberto *et al* [42], we calculate the atomic charges by integrating the DFT charge density inside the Voronoi cell of each atom. By definition, a point **r** belongs to the Voronoi cell of atom i if for all atoms j (j running over the nearest neighbors of atom i)

$$\frac{|\mathbf{r} - \mathbf{R}_i|}{b_i} < \frac{|\mathbf{r} - \mathbf{R}_j|}{b_j}, \qquad (1)$$

where $\mathbf{R}_{i(j)}$ and $b_{i(j)}$ stand for the position and coordination-dependent crystal radius [43] of atom $i(j)$. Table 2 gives the value used for each atomic coordination and the calculated atomic charge. We can see that as the coordination number of the cation increases, the ionic charge decreases, following the same trends found in γ-Al_2O_3 [39]. The average values obtained are 2.885 for Al and -1.923 for O. In the light of these results, we can argue that the average Al charge found in this work (2.885) represents an intermediate behavior between tetrahedral and octahedral bonding.

4. Concluding remarks

Structural analysis shows that the short-range order (up to 5 Å) is dominated by slightly distorted AlO_4 and AlO_5 units, together accounting for 90% of the basic units. The remaining 10% corresponds to AlO_6 units (octahedra). This fact is supported by the electronic structure analysis and in particular by the charge transfer along the Al–O bonds, which reveals a trend for decreasing ionic charge as the coordination number increases.

Structural analysis of intermediate-range order reveals two possible ways of linking the tetrahedral and octahedral basic units, namely, by corners or edges. This fact is supported by the results of vibrational analysis, which clearly highlight two different vibration bands having frequencies between 15 and 20 THz for the intra-unit modes and between 20 and 30 THz for the inter-unit modes.

Elastic properties such as the bulk and shear moduli were found to be consistently lower in amorphous alumina, as compared with the crystalline phases.

Acknowledgment

This work has been supported by grant Anillo *Computer simulation lab in nanobio systems* ACT-ADI 24/2006-Chile. SD acknowledges partial support from Fondecyt 3110017 and GG from ENL 10/06 VRID–Univ. de Chile.

References

[1] Wefers K and Misra C 1987 *Alcoa Technical Paper No.19* vol 50, p 770
[2] Wilk G D, Wallace R M and Anthony J M 2001 *J. Appl. Phys.* **89** 5243
[3] Momida H, Hamada T, Takagi Y, Yamamoto T, Uda T and Ohno T 2006 *Phys. Rev.* B **73** 054108
[4] Jin C, Zhou H and Wei W 2006 *Appl. Phys. Lett.* **89** 261103
[5] Stroud R M, Nittler L R and Alexander C M O D 2004 *Science* **305** 1455
[6] Demyk K, van Heijnsbergen D, von Helden G and Meijer G 2004 *Astron. Astrophys.* **420** 547
[7] Verhoelst T *et al* 2006 *Astron. Astrophys.* **447** 311
[8] Oka Y, Takahashi T, Okada K and Ichi Iwai S 1979 *J. Non-Cryst. Solids* **30** 349
[9] El-Mashri S M, Jones R G and Forty A J 1983 *Phil. Mag.* A **48** 665
[10] Lamparter P and Kniep R 1997 *Physica* B **234–236** 405
[11] Lee S K, Lee S B, Park S Y, Yi Y S and Ahn C W 2009 *Phys. Rev. Lett.* **103** 095501
[12] Lee S K, Park S Y, Yi Y S and Moon J 2010 *J. Phys. Chem.* C **114** 13890
[13] Sako S, Ohshima K and Fujita T 1990 *J. Phys. Soc. Japan* **59** 662
[14] Costina I and Franchy R 2001 *Appl. Phys. Lett.* **78** 4139
[15] Katiyar P, Jin C and Narayan R J 2005 *Acta Mater.* **53** 2617
[16] Benoit M, Ispas S, Jund P and Jullien R 2000 *Eur. Phys. J.* B **13** 631
[17] Giacomazzi L and Pasquarello A 2006 *Phys. Rev.* B **74** 155208
[18] Gutiérrez G and Johansson B 2002 *Phys. Rev.* B **65** 104202
[19] Matsui M 1994 *Miner. Mag.* A **58** 571
[20] Matsui M 1996 *Phys. Chem. Miner.* **23** 345
[21] Gutiérrez G, Belonoshko A B, Ahuja R and Johansson B 2000 *Phys. Rev.* E **61** 2723
[22] Kresse G and Hafner J 1994 *Phys. Rev.* B **49** 14251
[23] Kresse G and Furthmüller J 1996 *Phys. Rev.* B **54** 11169
[24] Kohn W 1999 *Rev. Mod. Phys.* **71** 1253
[25] Perdew J P and Zunger A 1981 *Phys. Rev.* B **23** 5048

[26] Vashishta P, Kalia R, Nakano A and Rino J P 2008 *J. Appl. Phys.* **108** 083504
[27] Hoang V V and Oh S K 2004 *Physica* B **352** 73
[28] A detailed comparison between classical and *ab initio* calculations regarding structural properties, can be found in Gutiérrez G *et al* 2010 *J. Mater. Sci.* **45** 5124–34
[29] Du J, Benmore C J, Corrales R, Hart R T and Weber J K R 2009 *J. Phys.: Condens. Matter* **21** 205102
[30] Jahn S and Madden P A 2007 *J. Non-Cryst. Solids* **353** 3500
[31] Birch F 1947 *Phys. Rev.* **71** 809
[32] Gutiérrez G, Taga A and Johansson B 2002 *Phys. Rev.* B **65** 012101
[33] Alcala G, Skeldon P, Thompson G E, Mann A B, Habazaki H and Shimizu K 2002 *Nanotechnology* **13** 451
[34] Xia Z, Sheldon B W, Curtin W A, Liang J, Yin A and Xu J M 2004 *Rev. Adv. Mater. Sci.* **6** 131
[35] Loong C K, Vashishta P, Kalia R K and Ebbsjo I 1995 *Europhys. Lett.* **31** 2001
[36] Sarnthein J, Pasquarello A and Car R 1997 *Science* **275** 1925
[37] Bell R J 1972 *Rep. Prog. Phys.* **35** 1315
[38] Lodziana Z and Parlinski K 2003 *Phys. Rev.* B **67** 174106
[39] Menéndez-Proupin E and Gutiérrez G 2005 *Phys. Rev.* B **72** 035116
[40] Ealet B, Elyakhlouffi M H, Gillet E and Ricci M 1994 *Thin Solid Films* **250** 92
[41] Savin A 2005 *J. Mol. Struct.: THEOCHEM* **727** 127
[42] Ruberto C, Yourdshahyan Y and Lundqvist B I 2003 *Phys. Rev.* B **67** 195412
[43] Shannon R D 1976 *Acta Crystallogr.* A **32** 751